Chinese Chemical Letters 31 (2020) 2757–2761

Contents lists available at ScienceDirect

Chinese Chemical Letters

journal homepage: www.elsevier.com/locate/cclet

Communication

Visible light induced efficient activation of persulfate by a carbon quantum dots (CQDs) modified γ-Fe_2O_3 catalyst

Yongjie Li[a,b,1], Wei Xiang[a,b,1], Tao Zhou[a,*], Mingjie Huang[a,*], Chen Wang[a,b], Xiaohui Wu[a,b], Juan Mao[a,b], Penghua Wang[c]

[a] School of Environmental Science and Engineering, Huazhong University of Science and Technology, Wuhan 430074, China
[b] Key Laboratory of Water and Wastewater Treatment (HUST), Ministry of Housing and Urban-Rural Development (MOHURD), Wuhan 430074, China
[c] Nanyang Environment & Water Research Institute (NEWRI), Nanyang Technological University, Singapore 637141, Singapore

ARTICLE INFO

Article history:
Received 11 December 2019
Received in revised form 24 December 2019
Accepted 15 January 2020
Available online 22 January 2020

Keywords:
Carbon quantum dots
Iron cycle
Photocatalysis
Persulfate

ABSTRACT

In this study, a carbon quantum dots modified maghemite catalyst (CQDs@γ-Fe_2O_3) has been synthesized by a one-step solvothermal method for efficient persulfate (PDS) activation under visible light irradiation. Transmission electron microscopy (TEM), scanning electron microscopy (SEM) and UV–vis diffuse reflectance spectroscopy (UV–vis DRS) characterization indicated that the formation of heterojunction structure between CQDs and γ-Fe_2O_3 effectively reduced the catalyst band gap (E_g), favoring the separation rate of electrons and holes, leading to remarkable efficient sulfamethoxazole (SMX) degradation as compared to the dark-CQDs@γ-Fe_2O_3/PDS and vis-γ-Fe_2O_3/PDS systems. The evolution of dissolved irons also demonstrated that CQDs could accelerate the *in-situ* reduction of surface-bounded Fe^{3+}. Electron paramagnetic resonance (EPR) and radical scavenging experiments demonstrated that both $^{\bullet}OH$ and $SO_4^{\bullet-}$ were generated in the reaction system, while $^{\bullet}OH$ was relatively more dominant than $SO_4^{\bullet-}$ for SMX degradation. Finally, the reaction mechanism in the vis-CQDs@γ-Fe_2O_3/PDS system was proposed involving an effective and accelerated heterogeneous-homogeneous iron cycle. CQDs would enrich the photo-generated electrons from γ-Fe_2O_3, causing efficient interfacial generation of surface-bond Fe^{2+} and reduction of adsorbed Fe^{3+}. This visible light induced iron cycle would eventually lead to effective activation of PDS as well as the efficient degradation of SMX.

As one of the typical pharmaceuticals and personal care products (PPCPs), sulfamethoxazole (SMX) has been widely used in human activities and frequently detected in effluents from municipal wastewater plants, the residual SMX in waters could cause potential negative effects on human health and the eco-environment [1]. Over the past decades, advanced oxidation processes (AOPs) based on the generation of highly reactive sulfate radical ($SO_4^{\bullet-}$) and hydroxyl radical ($^{\bullet}OH$) have been widely reported for effectively destructing recalcitrant PPCPs [2,3]. As compared to $^{\bullet}OH$, $SO_4^{\bullet-}$ presents advantages including higher oxidation potential (2.5–3.1 V) in a wide pH range and longer half-life (30–40 μs) [4]. Thus, $SO_4^{\bullet-}$ can better contact with target organics before self-quenching during the diffusion process [5]. It also reacts more selectively with the organic compounds containing unsaturated bonds or aromatic π electrons [6].

Usually, Different approaches have been used to activate persulfate (PS), such as increasing temperature, addition of transition metal or chelation agents, or by ultraviolet irradiation (UV) [7]. Among these, iron-based metal activation method was most studied and reported for efficient $SO_4^{\bullet-}$ production. And it has also been reported that heterogeneous catalysis with iron oxides are increasingly attractive in replacing homogeneous catalysis of persulfate to prevent the accumulation of soluble iron [8,9]. However, iron oxides present weak catalytic ability toward PS due to the slow solid-liquid interfacial mass transfer and low generation/regeneration of dissolved Fe^{2+} [10]. As a common semiconductor, the generation of photo-induced electron on the surface of iron oxides under the irradiation of UV light can also promote the PDS activation as well as the iron reduction. While the wide band width (E_g) and fast electron-hole recombination rate limit their practical use, further modification would be needed [11]. Recently, carbon-based materials have been widely used to enhance the visible light absorbance and electron transfer.

* Corresponding authors.
E-mail addresses: zhoutao@hust.edu.cn (T. Zhou), huangmingjie@hust.edu.cn (M. Huang).
[1] These authors contributed equally to this work.

https://doi.org/10.1016/j.cclet.2020.01.032
1001-8417/

Carbon quantum dots (CQDs) are of exclusive interest as an innovative family of materials for semiconductor photocatalysis for its low cost, upconversion ability and non-toxicity with reliable stability, as well as excellent electron-reservoir and electron-transfer properties [12]. It has been reported that CQDs could improve the photocatalytic activity of iron oxides by separating photogenerated charge carriers by forming heterojunction [13,14]. Recently, Zhang *et al.* investigated effective photocatalytic activity of Fe_2O_3/CQDs nanocomposites for the photodegradation of toxic gas (gas-phase benzene and methanol) under visible light and Zeinab Rabiei *et al.* investigated Ti/CQD@α-Fe_2O_3 photoanode for water splitting under visible light irradiation [15,16]. However, as far as we know, the photoactivation properties of PDS by CQDs modified iron oxide has not been studied yet.

In this study, a CQDs modified maghemite (γ-Fe_2O_3) catalyst was successfully synthesized by a one-step solvothermal method, which could efficiently activate PDS for rapid SMX degradation under visible light irradiation. The main objectives were to reveal the critical role of CQDs in improving the photochemical ability of the CQDs@γ-Fe_2O_3 catalyst and explore the reaction mechanism based on the enhanced solid-liquid interfacial iron cycle.

CQDs@γ-Fe_2O_3 was prepared by a one-step solvothermal synthesis method. Briefly, 0.8 g glucose (as precursor of carbon quantum dots) was dissolved in a 50 mL solution of ethanol:H_2O (1.5:1), then 5 g commercial γ-Fe_2O_3 (Aladdin Company) was dispersed in the mixed solution for 12 h, the above suspension was transferred to a 50 mL Teflon-lined stainless steel autoclave. The autoclave was heated at 180 °C for 24 h and then cooled to ambient temperature. The resulting precipitation was collected, washed, and vacuum dried at 60 °C.

Morphology of the CQDs@γ-Fe_2O_3 was characterized by a field emission-scanning electron microscopy (FE-SEM, EM3900 M, ZEISS, Germany) equipped with EDAX energy dispersive X-ray spectrometer (EDS) and a high-resolution transmission electron microscopy (HR-TEM, Tecnai G2 F30 transmission electron microscope). X-ray diffraction (XRD) was performed on a Seifert Iso-Debyeflex 2002 diffractometer using Cu–Kα radiation (wavelength =1.54 Å). The Brunauer-Emmett-Teller (BET) surface areas were obtained using a Gemini VII 2390 analyzer (Micromeritics Instrument Corp. U. S. A.). Zeta potentials were measured by a Zetasizer Nano-ZS90. The involved radicals were characterized by an electron paramagnetic resonance spectrometer (EPR, MEX-nano, Bruker), the modulation frequency was 100 kHz and the microwave power were 15 mW.

The photochemical degradation experiments of SMX were performed in a 500 mL jacket-glass reactor at 25 °C under the irradiation of a 300 W xenon lamp with light filter, which emitted visible light at 455 nm. In a typical experiment run, the reaction was started as adding 0.2 g/L of CQDs@γ-Fe_2O_3 into 500 mL reaction solution contain 10 mg/L SMX and 2 mmol/L PDS, the reaction pH was set to 3. Scavenging experiments were carried out in the presence of 500 mmol/L scavengers, *i.e. tert*-butyl alcohol (TBA), methanol (MeOH) and 10 mmol/L potassium bichromate ($K_2Cr_2O_7$), respectively.

Figs. 1a–c exhibited the SEM and TEM images of the CQDs@γ-Fe_2O_3 catalyst. It was found that the catalyst particles were uniform and agglomerative with a quasi-spheral morphology of 10−20 nm size, with evenly surface distribution of Fe, O and C. The lattice spacing of 0.220, 0.295 and 0.480 nm, corresponding to the (100) lattice of CQDs graphitic structure [17] and the (113) and (220) lattices of γ-Fe_2O_3 respectively [18], indicating heterojunction structure was formed between CQDs and γ-Fe_2O_3. It has been reported that the heterojunction structure could be benefit for the separation of photo-induced electron hole pair [19]. UV–vis Diffuse Reflectance Spectroscopy (UV–vis DRS) measurements revealed that the E_g of the CQDs/γ-Fe_2O_3 and γ-Fe_2O_3 were 2.40 and 2.51 eV, respectively, as shown in Fig. 1e. It indicated that CQDs could effectively improve the electron-hole separation efficiency under visible light irradiation. Fig. 1d showed the XRD patterns of γ-Fe_2O_3 and CQDs@γ-Fe_2O_3 nanoparticles. The diffraction peaks centered at $2\theta = 31.2°$, 33.9°, 44.1°, 52.5°, 57.6° and 63.9° were (220), (311), (400), (422), (511), and (440) planes of γ-Fe_2O_3 and CQDs@γ-Fe_2O_3, respectively. The strong peak at 18.1° corresponds to (100) lattice of CQDs graphitic structure in TEM, demonstrating that the fabricated catalyst was CQDs@γ-Fe_2O_3. The specific BET surface area of CQDs@γ-Fe_2O_3 increased dramatically after CQDs modification, reaching 101.2 m^2/g, four times higher than that of pristine γ-Fe_2O_3 (24.8 m^2/g). In Fig. 1f, the zeta potentials of

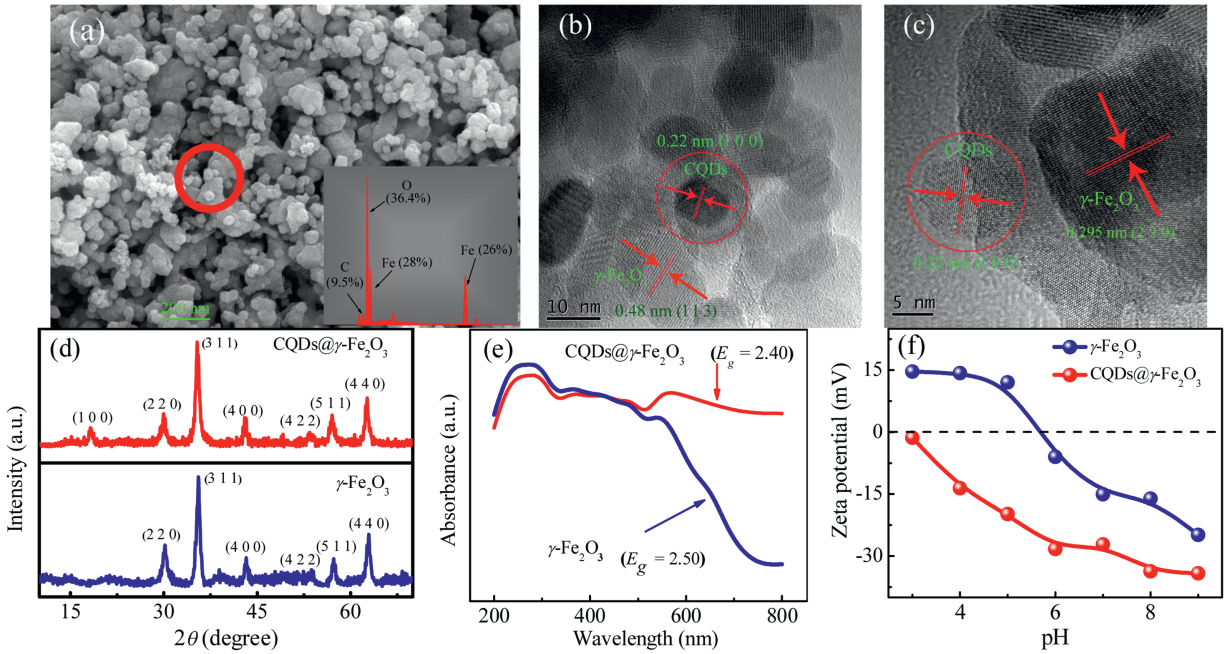

Fig. 1. (a) SEM-EDS, (b and c) HR-TEM and selected area electron diffraction images of CQDs@γ-Fe_2O_3, (d) XRD patterns, (e) UV–vis DRS spectra and (f) zeta potential measurements of γ-Fe_2O_3 and CQDs@γ-Fe_2O_3.

γ-Fe_2O_3 and CQDs@γ-Fe_2O_3 were also examined. The zeta potentials were 14.63 mV and −1.38 mV at pH 3 for γ-Fe_2O_3 and CQDs@γ-Fe_2O_3, respectively, indicating the different surface charge distribution properties of two catalysts. The negative charged surface of CQDs@γ-Fe_2O_3 at pH 3 means it could absorb more dissolved iron species, which was beneficial to the subsequence iron reduction and PDS activation. The transient photocurrent measurements were presented in Fig. S1 (Supporting information). It can be seen that the CQDs@γ-Fe_2O_3/PDS system possessed higher photocurrent density than the CQDs@γ-Fe_2O_3 system, indicating more photo-produced electrons were generated and transferred to PDS in the CQDs@γ-Fe_2O_3/PDS system.

Fig. 2a illustrated the time-dependent degradation of SMX in six comparative systems, *i.e.* vis-PDS, vis-CQDs@γ-Fe_2O_3, vis-γ-Fe_2O_3/PDS, vis-CQDs@γ-Fe_2O_3/PDS, dark-γ-Fe_2O_3/PDS and dark-CQDs@γ-Fe_2O_3/PDS systems. It was found that marginal SMX could be degraded in the vis-PDS, dark-γ-Fe_2O_3/PDS, indicating that PDS could not be activated by sole visible light or γ-Fe_2O_3. The poor SMX degradation in the vis-γ-Fe_2O_3/PDS system also demonstrated the weak photoresponse ability of γ-Fe_2O_3, perhaps due to the fast electron-hole recombination rate of γ-Fe_2O_3. Besides, Fig. 2b showed the vis-CQDs@γ-Fe_2O_3/PDS system could achieve much more rapid SMX degradation rate with a *pseudo* first-order kinetic constant (k_{obs}) of 1.6×10^{-2} min^{-1}, which was 8.0 and 31.8 times larger than of the dark-CQDs@γ-Fe_2O_3/PDS and vis-γ-Fe_2O_3/PDS systems, demonstrating that the loading of CQDs could greatly enhance the photocatalytic activity of the catalyst. As can be seen in the vis-CQDs@γ-Fe_2O_3 system, there was no SMX could be degraded in the absence of PDS, it proved that SMX could be degraded only when CQDs@γ-Fe_2O_3 activated PDS during visible light irradiation.

Figs. 2c and d shows the time-evolution of dissolved iron species in the γ-Fe_2O_3/PDS, CQDs@γ-Fe_2O_3 and CQDs@γ-Fe_2O_3/PDS systems with visible light irradiation or not. In the vis-γ-Fe_2O_3/PDS and dark-γ-Fe_2O_3/PDS systems, the time-dependent releases of iron species were both slight and Fe^{3+} would be the predominant iron species. It indicated that commercial γ-Fe_2O_3 would be hardly to photocatalytic activate PDS due to low generation/regeneration of Fe^{2+} [15]. Interestingly, the as-synthesized CQDs@γ-Fe_2O_3 could lead to relatively remarkable generation of dissolved Fe^{2+} up to about 2.5 mg/L at 120 min under visible light irradiation, while it leached about 2.4 mg/L Fe^{3+} and 0.3 mg/L Fe^{2+} in the corresponding dark case. Moreover, the concentration of Fe^{3+} would increase from 0 to 0.5 mg/L at the initial 40 min, but obviously decrease to 0.25 mg/L afterwards. This observation suggested that CQDs@γ-Fe_2O_3 would be visible light sensitive for effectively reductive generation of dissolved Fe^{2+} catalyst [19].

Apparently, similar dissolved amount of Fe^{2+}/Fe^{3+} were observed in the CQDs@γ-Fe_2O_3/PDS systems with visible light irradiation or not, while much more SMX was degraded in the vis-CQDs@γ-Fe_2O_3/PDS system (Fig. 2a). It indicated that more efficient iron cycles occurred under the co-effect of photo-induced electron reduction and PDS oxidation, leading to the generation of more reactive oxygen species (ROS) in the visible light irradiated system. Furthermore, it was interesting to note that evolution of total released dissolved iron in the four cases using CQDs@γ-Fe_2O_3 were almost similar with relatively low final amounts of about 2.6–2.7 mg/L. This result suggested that the introduction of CQDs would effectively improve the visible-activation performance of iron oxides materials and lead to acceleration in the solid-liquid interfacial iron cycle for efficient regeneration of Fe^{2+} [20]. In conclusion, the results of the iron evolution demonstrated that CQDs could greatly improve the photo-responsive behavior of γ-Fe_2O_3, leading to the faster separation rate of electron and hole. In this case, the photo-induced electrons could transfer to the surface of catalyst and contribute to the *in-situ* reduction of surface-bounded Fe^{3+} (Fig. 1f), thus, the more efficient iron cycle in

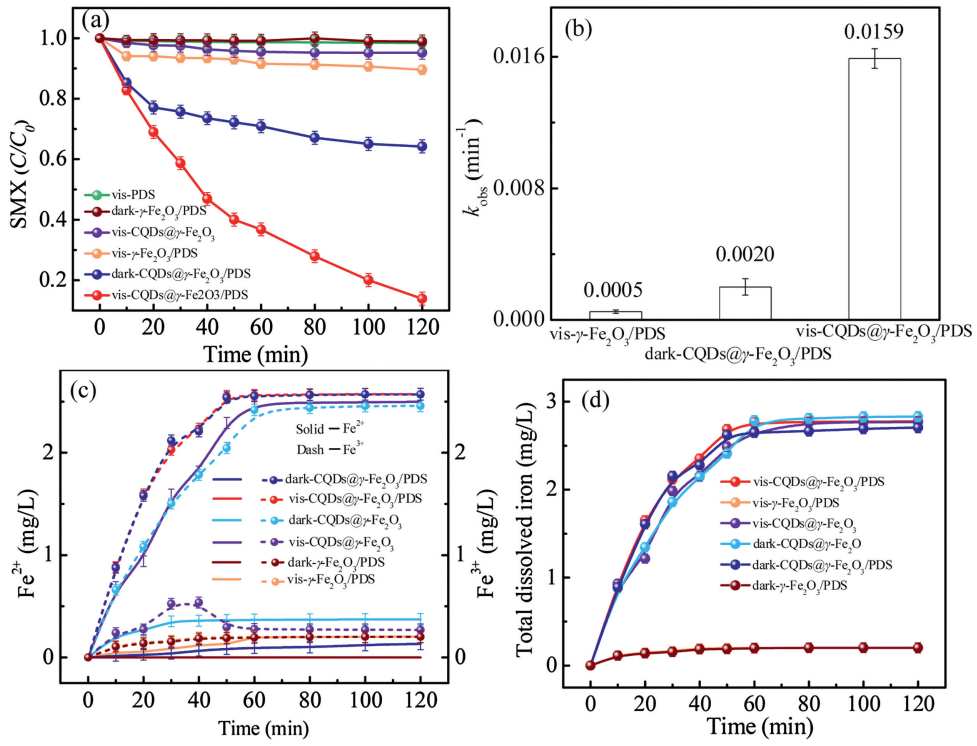

Fig. 2. (a) Comparative SMX degradation and (c) the corresponding simultaneous evolution of dissolved iron species in the vis-PDS, dark-γ-Fe_2O_3/PDS, vis-CQDs@γ-Fe_2O_3, vis-γ-Fe_2O_3/PDS, dark-CQDs@γ-Fe_2O_3/PDS and vis-CQDs@γ-Fe_2O_3/PDS systems. (b) The k_{obs} of SMX degradation and (d) release of total dissolved iron in the corresponding reaction systems. Initial conditions were: 0.2 g /L catalyst, 2 mmol/L PDS, 10 mg/L SMX, pH 3 and 25 °C.

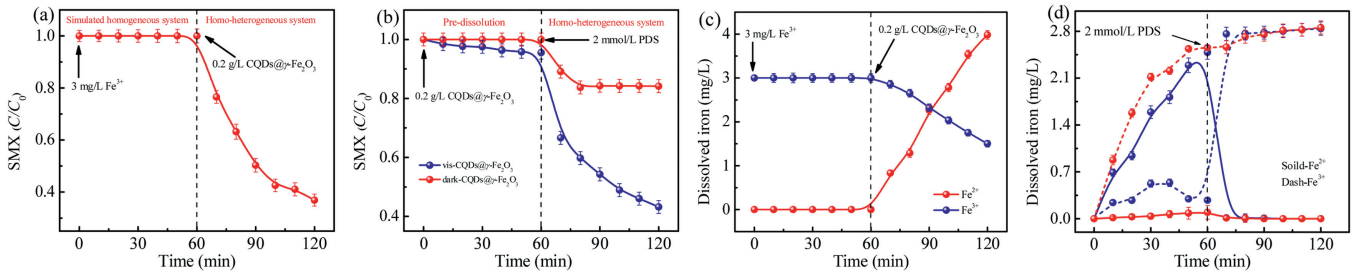

Fig. 3. (a) Degradation of SMX in a simulated homogeneous vis-Fe^{3+}(3 mg/L)/PDS system followed by adding 0.2 g/L CQDs@γ-Fe_2O_3 at 1 h. (b) Comparative degradation of SMX in the dark- and vis-CQDs@γ-Fe_2O_3/PDS systems after 1 h pre-dissolution under dark or visible light irradiation. (c) and (d) showed the evolution of dissolved iron species in the corresponding systems. Initial conditions were: 0.2 g/L CQDs@γ-Fe_2O_3, 10 mg/L SMX, pH 3 and 25 °C.

the CQDs@γ-Fe_2O_3/PDS system would lead to the faster degradation of SMX.

To further confirm the ROS involved in SMX degradation in the CQDs@γ-Fe_2O_3/PDS system, radical quenching and EPR experiments were conducted. As shown in Fig. S2a (Supporting information), the existence of either MeOH or TBA inhibited the degradation of SMX, with a dramatic decrease of k_{obs} from 1.6×10^{-2} min^{-1} to 4.0×10^{-4} min^{-1} and 1.4×10^{-3} min^{-1}, respectively. These results suggest that both $^{\bullet}OH$ and $SO_4^{\bullet-}$ were generated and took part in the reaction [21], while $^{\bullet}OH$ was relatively more dominant than $SO_4^{\bullet-}$ in the degradation process of SMX. Moreover, $K_2Cr_2O_7$, a scavenger for electrons [22], could entirely inhibit the SMX removal (Fig. S2a), indicating the crucial role of the photo-generated electrons for Fe^{3+} reduction and PDS activation. As depicted in Fig. S2b (Supporting information), the generation of $^{\bullet}OH$ and $SO_4^{\bullet-}$ in the vis-CQDs@γ-Fe_2O_3/PDS system were further confirmed by EPR study, notably, the extremely weak signal in the vis-CQDs@γ-Fe_2O_3 system indicated that PDS rather than O_2 was the source of ROS.

To further clarify the reaction mechanism in the vis-CQDs@γ-Fe_2O_3/PDS system, simulated homogeneous-heterogeneous systems were investigated. Fig. 3a presents the SMX degradation pattern in a homogeneous vis-Fe^{3+}(3 mg/L)/PDS system followed by adding 0.2 g/L CQDs@γ-Fe_2O_3 at 1 h. It can be seen that SMX could not be degraded in the homogeneous vis-Fe^{3+}/PDS, while 65% of SMX was removed after 1 h by adding CQDs@ γ-Fe_2O_3. Simultaneous evolution of dissolved iron in Fig. 3b revealed that CQDs@γ-Fe_2O_3 activated by visible light would effectively reduce the homogeneous Fe^{2+} and lead to rapid activation of PDS by Fe^{2+}.

Comparative degradation of SMX in the dark- and vis-CQDs@γ-Fe_2O_3/PDS systems was further investigated as shown in Fig. 3c, with 1 h pre-dissolution of 0.2 g/L CQDs@γ-Fe_2O_3/PDS under dark or visible light irradiation, respectively. Once PDS added, it was found that SMX could be rapidly degraded in the vis-CQDs@γ-Fe_2O_3/PDS system but slowly decomposed in the dark-system. The corresponding evolution of dissolved iron in Fig. 3d indicated that mainly release of Fe^{2+} from the dark dissolution of CQDs@γ-Fe_2O_3 would be responsible for the slow SMX degradation. However, visible prfeee-dissolution of CQDs@γ-Fe_2O_3 would lead to fast dissolved Fe^{2+}, causing the efficient activation of PDS for SMX degradation. In addition, the dissolved iron patterns presented similar evolution with almost Fe^{2+} in the vis- and dark- systems. Nevertheless, it was interesting to note that SMX could still be continuously degraded in the vis-CQDs@γ-Fe_2O_3/PDS system. This observation suggested that efficient interfacial regeneration of Fe^{2+} would occur based on the visible light irradiated CQDs@γ-Fe_2O_3. As the amount of PDS was enough, the regenerated Fe^{2+} would be fast consumed to produce $SO_4^{\bullet-}$.

The reusability of the catalysts is crucial in the practical application. To evaluate the catalytic stability of CQDs@γ-Fe_2O_3 catalyst, the particles were recovered to perform successive tests for SMX degradation (Fig. S3 in Supporting information). It can be seen that the recycled CQDs@γ-Fe_2O_3 catalyst showed strong activity in SMX degradation and its activity remained almost unchanged in six cycles.

The reaction mechanism in the vis-CQDs@γ-Fe_2O_3/PDS system was therefore proposed as presented in Fig. 4. The visible irradiation of CQDs@γ-Fe_2O_3 would be crucial for all the react included in the system. Advantages of the heterojunction structures of CQDs@γ-Fe_2O_3 would lead to the effective separation of photo-generated electrons and holes. Electrons would be enriched on the surface of CQDs, causing interfacial generation of surface-bond Fe^{2+} to activate PDS for SMX degradation. An efficient heterogeneous-homogeneous iron cycle would then occur

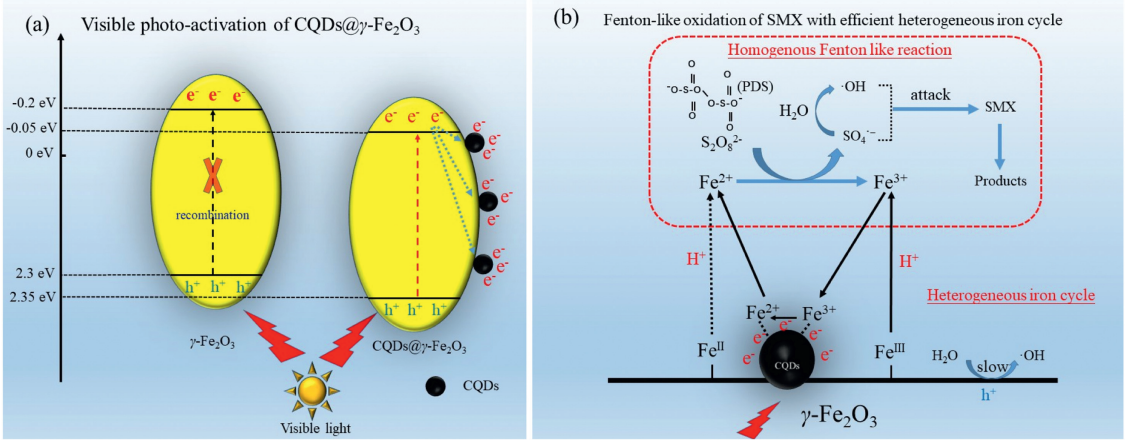

Fig. 4. Reaction mechanism in the vis-CQDs@γ-Fe_2O_3/PDS system.

in the vis-CQDs@γ-Fe_2O_3/PDS system. Fe^{2+} could be adsorbed on the CQDs surface and rapidly reduced to Fe^{2+}. Meanwhile, the regenerated Fe^{2+} would lead to the effective Fenton-like reaction of Fe^{2+}/PDS for continuous degradation of SMX.

The result of this study is expected to provide a novel and easily prepared photocatalyst for visible light activation of PDS. The advantage of CQDs@γ-Fe_2O_3 was revealed based on an efficient interfacial regeneration of Fe^{2+} by the photo-generated electrons. However, the electron transfer efficiency upon the specific iron oxides crystal lattices as well as the role of the separated holes are still needed to be further investigation.

Declaration of competing interest

The authors declare that they have no known competing financial interests or personal relationships that could have appeared to influence the work reported in this paper.

Acknowledgments

This study is financed by the National Natural Science Foundation of China (Nos. 21677055, 21407052), and the Fundamental Research Funds for the Central Universities, Huazhong University of Science and Technology (HUST) (Nos. 2017KFXKJC004, 2016YXMS287). Huazhong University of Science & Technology Analytic and Testing Centre is thanked for the advanced analytic operations.

Appendix A. Supplementary data

Supplementary material related to this article can be found, in the online version, at doi:https://doi.org/10.1016/j.cclet.2020.01.032.

References

[1] J. Wang, S. Wang, J. Environ. Manage. 182 (2016) 620–640.
[2] M. Huang, T. Zhou, X. Wu, J. Mao, Water Res. 119 (2017) 47–56.
[3] H. Zhang, Q. Ji, L. Lai, G. Yao, B. Lai, Chin. Chem. Lett. 30 (2019) 1129–1132.
[4] J. Li, Y. Wan, Y. Li, G. Yao, B. Lai, Appl. Catal. B: Environ. 256 (2019) 117782.
[5] F. Ghanbari, M. Moradi, Chem. Eng. J. 310 (2017) 42–62.
[6] Q. Zhao, Q. Mao, Y. Zhou, et al., Chemosphere 189 (2017) 224–238.
[7] A. Ghauch, A. Tuqan, N. Kibbi, Chem. Eng. J. 279 (2015) 861–873.
[8] Y. Lei, C. Chen, Y. Tu, Y. Huang, H. Zhang, Environ. Sci. Technol. 49 (2015) 6838–6845.
[9] C. Wang, Y. Liu, T. Zhou, et al., Chin. Chem. Lett. 30 (2019) 2231–2235.
[10] L. Wei, L. Zhu, W. Nan, et al., Environ. Sci. Technol. 44 (2010) 17–86.
[11] T. Zhou, X. Zou, X. Wu, J. Mao, J. Wang, Ultrason. Sonochem. 37 (2017) 320–327.
[12] Y. Guo, J. Zhang, D. Zhou, S. Dong, J. Mol. Liq. 262 (2018) 194–203.
[13] H. Zhou, Q. Sun, X. Wang, et al., Sep. Purif. Technol. 132 (2014) 346–353.
[14] F. Ghanbari, M. Moradi, Chem. Eng. J. 310 (2017) 41–62.
[15] L. Qiu, J. Ma, Sep. Purif. Technol. 210 (2018) 335–342.
[16] B. Yu, S. Kwak, J. Mater. Chem. 22 (2012) 8345–8353.
[17] S. Chandra, A. Chowdhuri, R. Angshuman, et al., J. Nanosci. Nanotechnol. 17 (2017) 1116–1124.
[18] X. Chen, X. Duan, W. Ou, et al., Appl. Catal. B 253 (2019) 419–432.
[19] M. Huang, W. Xiang, T. Zhou, et al., Sci. Total Environ. 697 (2019) 134220.
[20] X. Duan, S. Indrawirawan, J. Kang, et al., Sustain. Mater. Technol. 7 (2019) 23904–23913.
[21] K. Chung, C. Mei, J. Davies, K. Wilson, M. Chan, Atmos. Chem. Phys. 18 (2018) 2809–2820.
[22] G. Dong, L. Yang, F. Wang, ACS Catal. 6 (2016) 6511–6519.